Accuracy Assessment of Finite Volume Discretizations of Diffusive Fluxes on Unstructured Meshes

Conference Paper · January 2012

DOI: 10.2514/6.2012-608

2 authors:

Carl Frederick Ollivier-Gooch
University of British Columbia - Vancouver
159 PUBLICATIONS **2,809** CITATIONS

SEE PROFILE

Alireza Jalali
University of British Columbia - Vancouver
18 PUBLICATIONS **185** CITATIONS

SEE PROFILE

Accuracy Assessment of Finite Volume Discretizations of Diffusive Fluxes on Unstructured Meshes

Alireza Jalali*
Carl Ollivier-Gooch†
Department of Mechanical Engineering
The University of British Columbia
Vancouver, BC, V6T 1Z4, Canada

The results of the 3^{rd} AIAA Drag Prediction Workshop showed that numerical errors are comparable in magnitude to physical modeling errors. One route to reducing numerical errors is to improve discretization accuracy on a fixed mesh. This paper presents novel techniques for analysis of truncation error for finite-volume discretizations on unstructured meshes. We apply these techniques to compare the truncation error of discretization schemes commonly used for diffusive flux approximation in cell-centered finite volume solvers. For that purpose, two classes of tests are considered. Analytical tests on topologically regular meshes are done to eliminate those schemes that do not perform well even for slightly perturbed meshes. More complex numerical tests are conducted on the remaining schemes to extend the accuracy analysis to general unstructured meshes consisting of both isotropic and anisotropic triangles. We found that adding a solution jump term to the baseline face gradient (determined as the average of two adjacent cell gradients) reduces the truncation error for both isotropic and anisotropic test cases, while adding a finite difference correction term decreases the accuracy of discretization for isotropic grids. Also, a finite difference correction in the direction connecting cell centers does not affect the truncation error for anisotropic meshes.

I. Introduction

Accurate and reliable CFD simulation requires the ability to reduce and quantify both physical modeling errors (e.g. turbulence modeling) and numerical errors. The importance of the latter point is highlighted by the results of the 3^{rd} AIAA Drag Prediction Workshop which showed that the discretization error still is at least as large as other error sources and is more severe for unstructured flow solvers.[1] The local shape and connectivity of the mesh is more varied for unstructured meshes. Hence, it is more difficult to quantify discretization errors for them. In fact, mesh features — including cell size, anisotropy, shape, connectivity, and variations between adjacent cells — can have an adverse interaction with discretization schemes and this interaction may affect the solution accuracy. In spite of some recent research in this field, the interaction between mesh quality and discretization scheme and its impact on solution accuracy is not well understood for unstructured meshes.

Cary *et al*[2] introduced significant accuracy improvements in a turbulent flow solver by improving the cell gradient and viscous flux calculation, as well as the slope-limiter and boundary conditions implementations. They also described concisely an extensive family of schemes for calculating viscous fluxes on general unstructured meshes which have been used in the current research. Furthermore, Diskin *et al*,[3] compared the node-centered and cell-centered unstructured finite volume discretization schemes for viscous fluxes with the aim of improving turbulent simulations. This comparison was done on a range of grids from regular (structured) grids to irregular grids composed of arbitrary mixtures of triangles and quadrilaterals. The authors concluded that there is little difference in accuracy between node-centered schemes and the best

*M.Sc Student, arjalali@interchange.ubc.ca
†Professor, cfog@mech.ubc.ca, Member AIAA

cell-centered schemes, but poorly-designed cell-centered schemes behave much worse. Note that Diskin *et al* focus on cell-centered schemes that rely on a least-squares reconstruction of the solution at faces, as opposed to the cell-based reconstruction that we analyze here.

In this paper, we compare the accuracy of common second-order-accurate discretization schemes for calculating diffusive fluxes on unstructured meshes. In particular, we consider the Laplace equation as a model of viscous discretization and we use cell-centered finite volume approach. We describe in Section II a number of discretization schemes which differ in how cell gradients are combined to compute a face gradient; in the presence and form of finite difference correction terms to the gradient; and in treatment of the discontinuity at faces. These schemes are tested on unstructured grids to study the effect of mesh features and discretization schemes on accuracy. Two classes of tests are considered. The first class of tests, discussed in Section III, is an analytical test on both uniform and distorted triangular meshes, using a simple geometric generalization of the analysis technique of Ollivier-Gooch and van Altena.[4] The distorted meshes are produced by shearing, scaling, stretching, curving and random perturbation of the uniform mesh. The goal of this analytical test is to investigate the accuracy of both cell gradient and flux integral by obtaining their truncation error coefficients. In this way, it is possible to evaluate the the accuracy of a specific discretization scheme for slightly disturbed meshes. The more effective scheme is defined as the scheme which produces less truncation error in the flux integral. Those schemes that perform well for distorted meshes are selected and used in the second class of tests, discussed in Section IV. These numerical tests extend the investigation of appropriate discretization schemes to general unstructured meshes. Numerical tests combine the Jacobian of the discretization scheme and a series expansion of control volume averages to find the coefficients in the truncation error for general meshes. This section provides numerical results obtained through the implementation of effective discretization schemes to both isotropic and anisotropic unstructured test cases. Finally, Section V contains a summary and some concluding remarks.

II. Discretization Schemes

This section discusses unstructured grid cell gradient calculation and reviews several approaches for using cell gradients to compute the face gradients necessary for diffusive fluxes.

A. Cell gradient calculation

Calculating the diffusive fluxes for Laplace's equation, $\nabla^2\phi = 0$, requires the solution gradients at the cell interfaces. To obtain the face gradient, the gradient for the cells on either side of it should be computed in terms of control volume averages. Therefore, a solution reconstruction process is needed to replace the control volume averaged value of the solution $\overline{\phi}_i$ with a Taylor series expansion of solution around the reference point.

$$\begin{aligned}\phi_i^R(x-x_i, y-y_i) &= \phi|_i + \left.\frac{\partial\phi}{\partial x}\right|_i (x-x_i) + \left.\frac{\partial\phi}{\partial y}\right|_i (y-y_i) + \left.\frac{\partial^2\phi}{\partial x^2}\right|_i \frac{(x-x_i)^2}{2} \\ &\quad + \left.\frac{\partial^2\phi}{\partial x\partial y}\right|_i (x-x_i)(y-y_i) + \left.\frac{\partial^2\phi}{\partial y^2}\right|_i \frac{(y-y_i)^2}{2} + \ldots \end{aligned} \tag{1}$$

In Equation 1, ϕ_i is the value of reconstructed solution and $\frac{\partial^{k+l}\phi_i}{\partial x^k \partial y^l}$ are its derivatives at the reference point of control volume i.

Conservation of the mean within a control volume requires that

$$\frac{1}{A_i}\int_{V_i} \phi_i^R dA = \overline{\phi}_i \tag{2}$$

By expanding the left-hand side of Equation 2 term by term, one can easily show that

$$\frac{1}{A_i}\int_{V_i} \phi_i^R dA = \phi|_i + \left.\frac{\partial\phi}{\partial x}\right|_i \overline{x}_i + \left.\frac{\partial\phi}{\partial y}\right|_i \overline{y}_i + \left.\frac{\partial^2\phi}{\partial x^2}\right|_i \frac{\overline{x^2}_i}{2} + \left.\frac{\partial^2\phi}{\partial x\partial y}\right|_i \overline{xy}_i + \left.\frac{\partial^2\phi}{\partial y^2}\right|_i \frac{\overline{y^2}_i}{2} + \ldots \tag{3}$$

where

$$\overline{x^n y^m}_i = \frac{1}{A_i}\int_{V_i} (x-x_i)^n (y-y_i)^m dA. \tag{4}$$

Considering Equation 3 reveals that $\overline{\phi}_i = \phi_i$ for a second-order scheme if the cell centroid is chosen as the reference point. For a second-order scheme, it is necessary to calculate the gradient vector for each control volume. In this paper, both least-squares reconstruction and the Green-Gauss method have been used to obtain the cell gradients.

1. Least-squares reconstruction for gradient calculation

In this method, the cell gradient is computed by minimizing the error in predicting the mean value of the reconstructed solution for control volumes in the stencil $\{V_j\}_i$. In other words, the difference between the actual control volume average $\overline{\phi}_j$ and the average of ϕ_i^R over control volume j is minimized.[4] The mean value for a single control volume V_j of the reconstructed solution ϕ_i^R is

$$\begin{aligned}\frac{1}{A_j}\int_{V_j}\phi_i^R dA &= \phi|_i + \left.\frac{\partial\phi}{\partial x}\right|_i \left\{\frac{1}{A_j}\int_{V_j}(x-x_i)\,dA\right\} + \left.\frac{\partial\phi}{\partial y}\right|_i \left\{\frac{1}{A_j}\int_{V_j}(y-y_i)\,dA\right\} \\ &+ \left.\frac{\partial^2\phi}{\partial x^2}\right|_i \left\{\frac{1}{2A_j}\int_{V_j}(x-x_i)^2\,dA\right\} \\ &+ \left.\frac{\partial^2\phi}{\partial x\partial y}\right|_i \left\{\frac{1}{A_j}\int_{V_j}(x-x_i)(y-y_i)\,dA\right\} \\ &+ \left.\frac{\partial^2\phi}{\partial y^2}\right|_i \left\{\frac{1}{2A_j}\int_{V_j}(y-y_i)^2\,dA\right\} + ... \end{aligned} \tag{5}$$

To avoid computing moments of each control volume in $\{V_j\}_i$ about the reference point of control volume i, replace $x - x_i$ and $y - y_i$ with $(x - x_j) + (x_j - x_i)$ and $(y - y_j) + (y_j - y_i)$, respectively. Using Equation 4, we obtain

$$\begin{aligned}\frac{1}{A_j}\int_{V_j}\phi_i^R dA &= \phi_i + \left.\frac{\partial\phi}{\partial x}\right|_i (\overline{x}_j + (x_j - x_i)) + \left.\frac{\partial\phi}{\partial y}\right|_i (\overline{y}_j + (y_j - y_i)) \\ &+ \left.\frac{\partial^2\phi}{\partial x^2}\right|_i \left(\frac{\overline{x^2}_j + 2\overline{x}_j(x_j - x_i) + (x_j - x_i)^2}{2}\right) \\ &+ \left.\frac{\partial^2\phi}{\partial x\partial y}\right|_i (\overline{xy}_j + \overline{x}_j(y_j - y_i) + (x_j - x_i)\overline{y}_j + (x_j - x_i)(y_j - y_i)) \\ &+ \left.\frac{\partial^2\phi}{\partial y^2}\right|_i \left(\frac{\overline{y^2}_j + 2\overline{y}_j(y_j - y_i) + (y_j - y_i)^2}{2}\right) + ... \end{aligned} \tag{6}$$

This equation is written for every control volume within the stencil of control volume i. The number of these control volumes must be more than two to yield a least-squares system which gives the value of the first derivatives. In this paper, control volumes within the stencil are chosen to be those three triangular cells which are the face neighbors of the target cell.

Setting the reference point of each cell as its centroid, $\overline{x}_i = \overline{x}_j = \overline{y}_i = \overline{y}_j = 0$ in Equation 6. Therefore, the least-squares system for linear reconstruction becomes:

$$\begin{bmatrix} w_{i1}(x_1 - x_i) & w_{i1}(y_1 - y_i) \\ w_{i2}(x_2 - x_i) & w_{i2}(y_2 - y_i) \\ w_{i3}(x_3 - x_i) & w_{i3}(y_3 - y_i) \end{bmatrix} \begin{pmatrix} \frac{\partial\phi}{\partial x} \\ \\ \frac{\partial\phi}{\partial y} \end{pmatrix}_i = \begin{pmatrix} w_{i1}(\overline{\phi}_1 - \overline{\phi}_i) \\ w_{i2}(\overline{\phi}_2 - \overline{\phi}_i) \\ w_{i3}(\overline{\phi}_3 - \overline{\phi}_i) \end{pmatrix} \tag{7}$$

In Equation 7 the weights are set to emphasize geometrically nearby data:

$$w_{ij} = \frac{1}{|\vec{r}_j - \vec{r}_i|} \tag{8}$$

where $\vec{r}$ is the position vector for each cell reference point.

2. Green-Gauss theorem for gradient calculation

Another common approach to calculate the solution gradient in a second-order scheme is to take advantage of the Green-Gauss theorem which states that the surface integral of a scalar function is equal to the volume integral of the gradient of the scalar function over the volume bounded by the surface:

$$\nabla\phi_i A_i \equiv \int_{V_i} \nabla\phi \, dA = \oint_{\partial V} \phi \, \hat{n} \, ds \tag{9}$$

The right-hand side of Equation 9 can be approximated to second order accuracy, by the summation of the average face values. In the present case, the average face values are obtained by an inverse distance weighted average between the cell-center values that share the face.

$$\nabla\phi_i = \frac{1}{A_i} \sum_{k=1}^{3} \overline{\phi}_k \hat{n}_k s_k, \qquad \overline{\phi}_k = \frac{|\vec{r}_{jF}| \, \overline{\phi}_i + |\vec{r}_{iF}| \, \overline{\phi}_j}{|\vec{r}_{iF}| + |\vec{r}_{jF}|} \tag{10}$$

where $\overline{\phi}_k$ is the average face value, $\hat{n}_k$ and s_k are the outward unit normal vector and the length of the corresponding face, $\overline{\phi}_i$ is the control volume average value of the cell whose gradient is being calculated, $\overline{\phi}_j$ is the control volume average value in the neighboring cell j, $\vec{r}_{iF}$ is the vector from the cell i to the face center, and $\vec{r}_{jF}$ is the vector from the face neighbor cell center to face center (see Figure 1).

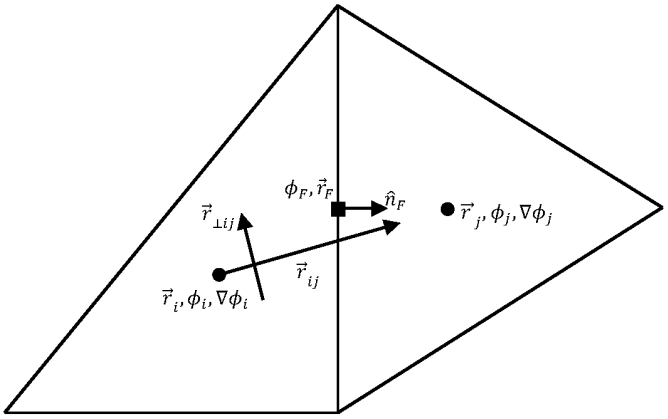

Figure 1: Mesh geometric properties

B. Face gradient calculation

The calculation of viscous fluxes requires estimates of solution gradients at the face center. Even though for a structured scheme, a central differencing is usually used, this approach is problematical for unstructured grids, because the cell centroids are often far from lying on the perpendicular bisector of the face between them. Many unstructured finite-volume solvers use a combination of averaging the cell gradient with a finite difference across the face.[3,5] In addition, a jump term which comes from the discontinuous solution at the face center is sometimes added to the face gradient. These variations are described in detail by Cary et al.[2] The baseline face gradient is determined first by averaging the cell center gradients obtained by using least squares or Green-Gauss. Then, a finite difference correction can be applied by replacing the component of face gradient in either the face normal direction or along the line between the cell centers with a finite difference term while retaining the cell center averaged gradient in the perpendicular direction. Finally, a jump term (discussed in detail by Nishikawa[6]), in the face normal direction, may be added to

take into account the effect of solution discontinuity at the face center. In the jump term formulation, α is an arbitrary value which is called the jump term coefficient. Methods are described by an alphanumeric triplet according to the keys listed in Table 1 that indicates the averaging, finite difference correction used (if any), and whether the jump condition is used. For instance, "VEJ" is deciphered as a scheme in which a volume-weighted average is performed of the cell center gradients. Then the finite difference component in the direction of the line connecting the cell-centers is computed. The averaged gradient is projected onto the direction perpendicular to the line connecting the cell centers and added to the finite difference term. Finally, the jump term is added to yield the face gradient used in the flux integration. Mathematically, this can be written as

$$\begin{aligned}(\nabla\phi)_{VEJ} &= \left(\frac{A_i}{A_i+A_j}\nabla\phi_i + \frac{A_j}{A_i+A_j}\nabla\phi_j\right)\cdot\vec{r}_{\perp ij}\frac{\vec{r}_{\perp ij}}{|\vec{r}_{\perp ij}|} \\ &+ \left(\frac{\vec{r}_{ij}}{|\vec{r}_{ij}|^2}\left(\overline{\phi}_j - \overline{\phi}_i\right)\right) + \left(\frac{\alpha}{|\vec{r}_{ij}.\hat{n}_F|}\left(\phi_{F^+} - \phi_{F^-}\right)\hat{n}_F\right)\end{aligned} \tag{11}$$

For schemes in which a finite difference correction is not used, the averaged cell center gradient is added to the jump term. For example, Equation 12 gives the face gradient for the "A0J" scheme.

$$(\nabla\phi)_{A0J} = \left(\frac{1}{2}\nabla\phi_i + \frac{1}{2}\nabla\phi_j\right) + \left(\frac{\alpha}{|\vec{r}_{ij}.\hat{n}_F|}\left(\phi_{F^+} - \phi_{F^-}\right)\hat{n}_F\right) \tag{12}$$

Key	Explanation	Formula
	Cell Gradient Averaging	
0	No Cell Averaging	—
A	Arithmetic Averaging	$\frac{1}{2}\nabla\phi_i + \frac{1}{2}\nabla\phi_j$
V	Volume-Weighted	$\frac{A_i}{A_i+A_j}\nabla\phi_i + \frac{A_j}{A_i+A_j}\nabla\phi_j$
L	Linear Interpolation	$\frac{\left\vert\vec{r}_{jF}\right\vert}{\vert\vec{r}_{iF}\vert+\left\vert\vec{r}_{jF}\right\vert}\nabla\phi_i + \frac{\vert\vec{r}_{iF}\vert}{\vert\vec{r}_{iF}\vert+\left\vert\vec{r}_{jF}\right\vert}\nabla\phi_j$
	Finite Difference Correction	
0	No Finite Difference	—
E	Cell-Center "Edge" Direction	$\frac{\vec{r}_{ij}}{\vert\vec{r}_{ij}\vert^2}\left(\phi_j - \phi_i\right)$
N	Face Normal Direction	$\frac{1}{\hat{n}_F.\vec{r}_{ij}}\left(\phi_j - \phi_i\right)\hat{n}_F$
C	Corrected Normal Direction	$\frac{1}{\hat{n}_F.\vec{r}_{ij}}\left(\phi_j - \phi_i + \left(\nabla\phi_j.\vec{t}_F\right)\left(\vec{r}_{jF}.\vec{t}_F\right) - \left(\nabla\phi_i.\vec{t}_F\right)\left(\vec{r}_{iF}.\vec{t}_F\right)\right)$
	Face Discontinuity Correction	
0	No Jump Term	—
J	Jump Term	$\frac{\alpha}{\left\vert\vec{r}_{ij}.\hat{n}_F\right\vert}\left(\phi_{F^+} - \phi_{F^-}\right)\hat{n}_F$

Table 1: Face gradient component

III. Analytic Tests

To investigate the accuracy of discretization schemes on unstructured mesh, we begin with the analysis of truncation error of cell gradient and flux integral for uniform and distorted meshes. For uniform meshes, most common schemes are identical; the aim of this experiment is to eliminate the schemes whose accuracy degrades excessively for slightly distorted meshes. The results will guide our numerical experiments on genuinely unstructured meshes.

A. Mesh distortion definitions

Our analytic tests use five families of distorted meshes created by disturbing the vertices of a uniform triangular mesh. Figure 2a shows the geometry and numbering order for uniform mesh. This kind of mesh

consists of equilateral triangles whose edges have length h. Accuracy assessments in terms of cell gradient and flux integral errors are done for control volume 1, CV_1. Therefore, the centroid of CV_1 is chosen as the coordinate system origin. We keep this origin for all of the distorted meshes for consistency. In other words, the triangles vertices are perturbed so that the centroid of CV_1 stays at the origin.

Five types of distortion are considered:

1. *Sheared meshes*, in which the y-coordinates of vertices are unchanged and all vertices in each horizontal line in the mesh are shifted horizontally by the same amount. The new x-coordinates of points are specified based on their y-coordinate so that the slanted lines in the mesh remain straight and parallel. Figure 2b shows the sheared mesh. This type of mesh is quantified by a shearing factor b, which is zero for an equilateral mesh and $\frac{1}{3}$ for a mesh of right triangles.

2. *Scaled meshes*, in which the x-coordinates of the uniform mesh vertices are kept and their y-coordinates are scaled by a factor of k, as seen in Figure 2c.

3. *Stretched meshes,* in which the x-coordinates of vertices are again identical to the uniform mesh and the y-coordinates of points are disturbed. In this type of mesh, a non-uniform distortion is applied, introducing variation in size and shape between cells sharing a face. In this sense, this mesh is more similar to general unstructured meshes. This mesh is quantified by a stretching factor s that controls the height of each row. The center row of mesh contains isotropic triangles while lower and upper rows have smaller and larger aspect ratios, respectively (see Figure 2d).

4. *Curved meshes*, in which the mesh vertices are transformed to a radial coordinate system. Vertices in the same horizontal line (same y-coordinate) in the uniform mesh have the same radial coordinate in the distorted mesh, while vertices with the same x-coordinate in the uniform mesh are on the same radial line (θ-coordinate); see Figure 2e. These meshes are characterized by the (constant) ratio R between the radius at consecutive mesh lines and by the aspect ratio a of the triangles.

5. *Randomly perturbed meshes,* in which both coordinates of the uniform mesh vertices are randomly shifted by a factor of εh, where $\varepsilon \in [-0.1, 0.1]$. Then, the vertices are all translated so that the the centroid of CV_1 coincides with the origin (see Figure 2f).

B. Cell gradient

Since the computation of viscous fluxes requires the calculation of cell gradients, the accuracy of the method by which the cell gradient is approximated affects the overall accuracy of the scheme. Using either the least-squares method (Equation 7) or the Green-Gauss theorem (Equation 10), the cell gradient of an arbitrary control volume (here CV_1) is calculated in terms of control volume averages of itself and its neighbors. For example, using the least-squares method for computing the cell gradient of a uniform mesh results in

$$\widetilde{\nabla}\phi_1 = \begin{pmatrix} \widetilde{\frac{\partial\phi}{\partial x}} \\ \\ \widetilde{\frac{\partial\phi}{\partial y}} \end{pmatrix}_1 = \begin{pmatrix} \frac{1}{h}\left(\overline{\phi}_3 - \overline{\phi}_2\right) \\ \\ \frac{\sqrt{3}}{3h}\left(\overline{\phi}_2 + \overline{\phi}_3 - 2\overline{\phi}_4\right) \end{pmatrix} \tag{13}$$

We can expand the control volume averages in terms of derivatives of an underlying smooth solution ϕ at the centroid of CV_1 by using Equation 6. Therefore, the control volume averages in Equation 13 can be computed as

$$\begin{aligned} \overline{\phi}_2 &= \phi_1 + h\left(-\frac{1}{2}\left.\frac{\partial\phi}{\partial x}\right|_1 + \frac{\sqrt{3}}{6}\left.\frac{\partial\phi}{\partial y}\right|_1\right) + \\ &\quad h^2\left(\frac{7}{48}\left.\frac{\partial^2\phi}{\partial x^2}\right|_1 - \frac{1}{12}\left.\frac{\partial^2\phi}{\partial x\partial y}\right|_1 + \frac{1}{16}\left.\frac{\partial^2\phi}{\partial y^2}\right|_1\right) + \mathcal{O}(h^3) \\ \overline{\phi}_3 &= \phi_1 + h\left(\frac{1}{2}\left.\frac{\partial\phi}{\partial x}\right|_1 + \frac{\sqrt{3}}{6}\left.\frac{\partial\phi}{\partial y}\right|_1\right) + \end{aligned} \tag{14}$$

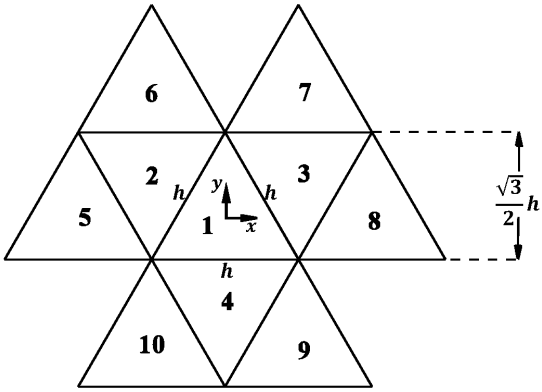

(a) Uniform mesh

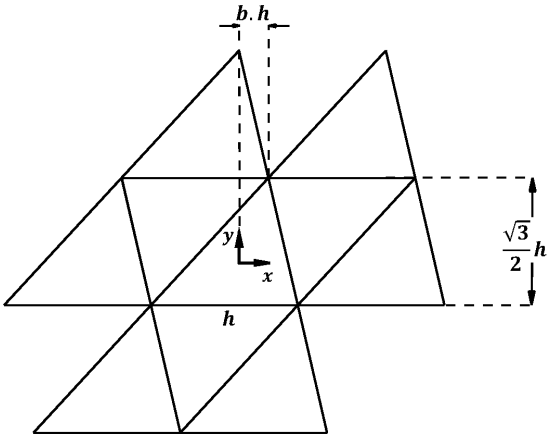

(b) Sheared mesh

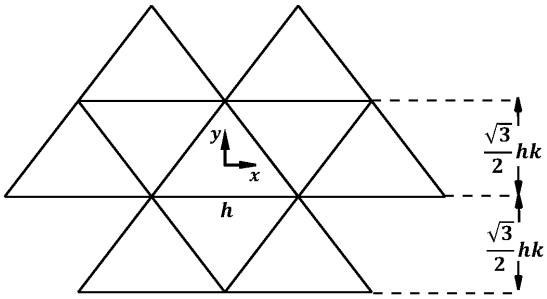

(c) Scaled mesh

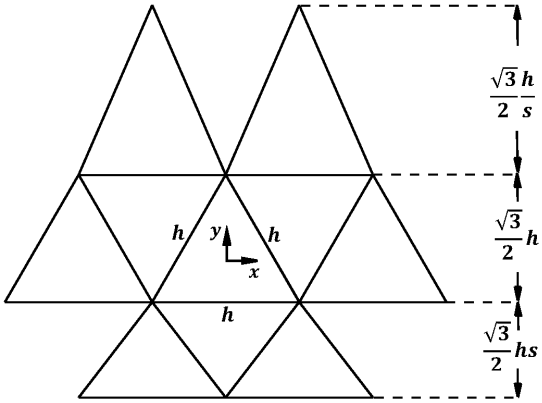

(d) Stretched mesh

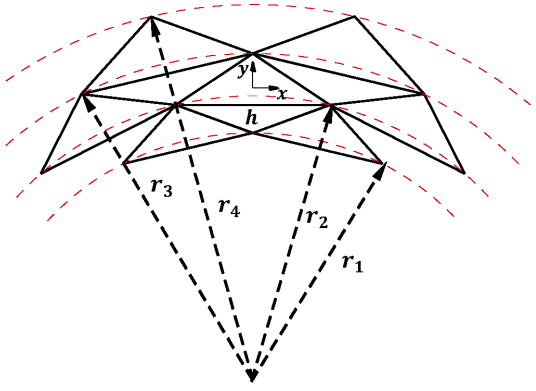

(e) Curved mesh

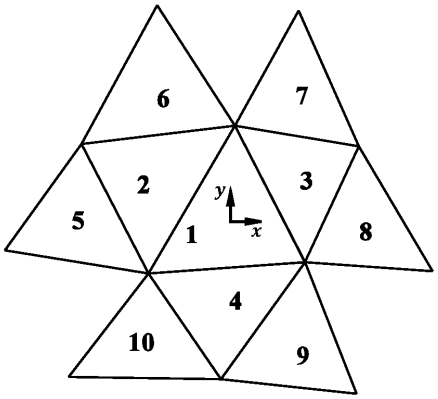

(f) Randomly perturbed mesh

Figure 2: Uniform and distorted meshes for analytic tests.

$$
\begin{aligned}
& h^2 \left(\frac{7}{48} \left.\frac{\partial^2 \phi}{\partial x^2}\right|_1 + \frac{1}{12} \left.\frac{\partial^2 \phi}{\partial x \partial y}\right|_1 + \frac{1}{16} \left.\frac{\partial^2 \phi}{\partial y^2}\right|_1 \right) + \mathcal{O}(h^3) \\
\overline{\phi}_4 \;=\; & \phi_1 + h \left(-\frac{\sqrt{3}}{3} \left.\frac{\partial \phi}{\partial y}\right|_1 \right) + \\
& h^2 \left(\frac{1}{48} \left.\frac{\partial^2 \phi}{\partial x^2}\right|_1 + \frac{3}{16} \left.\frac{\partial^2 \phi}{\partial y^2}\right|_1 \right) + \mathcal{O}(h^3)
\end{aligned}
$$

Also, the control volume average of the actual gradient for an arbitrary control volume is obtained as

$$
\overline{\nabla \phi}_i = \begin{pmatrix} \overline{\frac{\partial \phi}{\partial x}} \\ \\ \overline{\frac{\partial \phi}{\partial y}} \end{pmatrix}_i = \begin{pmatrix} \left.\frac{\partial \phi}{\partial x}\right|_i + \left.\frac{\partial^2 \phi}{\partial x^2}\right|_i \overline{x}_i + \left.\frac{\partial^2 \phi}{\partial x \partial y}\right|_i \overline{y}_i + \ldots \\ \\ \left.\frac{\partial \phi}{\partial y}\right|_i + \left.\frac{\partial^2 \phi}{\partial x \partial y}\right|_i \overline{x}_i + \left.\frac{\partial^2 \phi}{\partial y^2}\right|_i \overline{y}_i + \ldots \end{pmatrix} \tag{15}
$$

Substituting the control volume averages in $\widetilde{\nabla \phi}_1$ with the expansions of Equation 14, the difference between the computed gradient, $\widetilde{\nabla \phi}_1$ and the control volume average of the actual gradient $\overline{\nabla \phi}_1$ yields the the cell gradient truncation error. The general form of this error is

$$
\widetilde{\nabla \phi}_1 - \overline{\nabla \phi}_1 = \begin{pmatrix} \left(\alpha_x \left.\frac{\partial \phi}{\partial x}\right|_1 + \alpha_y \left.\frac{\partial \phi}{\partial y}\right|_1 \right) + \\ h \left(\alpha_{xx} \left.\frac{\partial^2 \phi}{\partial x^2}\right|_1 + \alpha_{xy} \left.\frac{\partial^2 \phi}{\partial x \partial y}\right|_1 + \alpha_{yy} \left.\frac{\partial^2 \phi}{\partial y^2}\right|_1 \right) + \mathcal{O}\left(h^2\right) \\ \\ \left(\beta_x \left.\frac{\partial \phi}{\partial x}\right|_1 + \beta_y \left.\frac{\partial \phi}{\partial y}\right|_1 \right) + \\ h \left(\beta_{xx} \left.\frac{\partial^2 \phi}{\partial x^2}\right|_1 + \beta_{xy} \left.\frac{\partial^2 \phi}{\partial x \partial y}\right|_1 + \beta_{yy} \left.\frac{\partial^2 \phi}{\partial y^2}\right|_1 \right) + \mathcal{O}\left(h^2\right) \end{pmatrix} \tag{16}
$$

Table 2 gives the coefficients in Equation 16 for the gradient calculations shown above. The least-squares and Green-Gauss gradients are identical (and first-order accurate) for the uniform mesh, but the accuracy of the cell gradient is reduced by one order using Green-Gauss for a randomly perturbed mesh. The least-squares method produces a first-order gradient ($\alpha_x = \alpha_y = 0$ and $\beta_x = \beta_y = 0$) for the randomly perturbed mesh which implies a second-order solution reconstruction, whereas the Green-Gauss method gives a zero-order cell gradient[a]. Since the utilized perturbation just results in a slightly distorted grid, we conclude Green-Gauss is not a reliably accurate method for cell gradient calculation of general unstructured meshes. Therefore, only least-squares approximation will be used for numerical tests of general meshes in Section IV.

C. Flux integral

Having computed the cell gradient through the least-squares method and using different discretization schemes discussed in Section II for evaluation of the face gradient, the flux integral can be computed using

$$
\widetilde{\nabla^2 \phi_i} = \frac{1}{A_i} \oint_{\partial V_i} \nabla \phi \cdot \vec{ds} \tag{17}
$$

By computing the flux integral for CV_1, we obtain an expression for the computed Laplacian $\widetilde{\nabla^2 \phi_1}$ based on control volume averages. The computed Laplacian is a linear combination of 10 control volumes averages (CV_1–CV_{10}) in the stencil. Equation 18 shows such a relation for the computed Laplacian of CV_1 using the uniform mesh and the $A00$ discretization scheme.

$$
\widetilde{\nabla^2 \phi_1} = -\frac{1}{3h^2} (12 \overline{\phi}_1 - 2 \sum_{j=5}^{10} \overline{\phi}_j) \tag{18}
$$

[a] At least as formulated in Section 2; more than one Green-Gauss formulation is possible.

Mesh	α_x	α_y	α_{xx}	α_{xy}	α_{yy}
			Least Squares		
Uniform	0	0	0	$\frac{\sqrt{3}}{6}$	0
Randomly perturbed	0	0	−0.030961	0.261269	−0.000665
			Green-Gauss		
Uniform	0	0	0	$\frac{\sqrt{3}}{6}$	0
Randomly perturbed	0.016043	−0.008842	−0.015702	0.267364	0.016791

(a) Truncation error coefficients of $\frac{\partial \phi}{\partial x}$

Mesh	β_x	β_y	β_{xx}	β_{xy}	β_{yy}
			Least Squares		
Uniform	0	0	$\frac{\sqrt{3}}{12}$	0	$-\frac{\sqrt{3}}{12}$
Randomly perturbed	0	0	0.137161	−0.030569	−0.139801
			Green-Gauss		
Uniform	0	0	$\frac{\sqrt{3}}{12}$	0	$-\frac{\sqrt{3}}{12}$
Randomly perturbed	0.000740	−0.014895	0.132207	−0.030198	−0.140482

(b) Truncation error coefficients of $\frac{\partial \phi}{\partial y}$

Table 2: Cell gradient truncation error coefficients

Expanding control volume averages in $\widetilde{\nabla^2 \phi_1}$ in terms of derivatives of the underlying smooth solution ϕ at the origin and computing $\overline{\nabla^2 \phi}_1$ yields the flux integral truncation error, written in general form as:

$$\begin{aligned} \widetilde{\nabla^2 \phi_1} - \overline{\nabla^2 \phi}_1 \quad = \quad & \left(\lambda_{xx} \left. \frac{\partial^2 \phi}{\partial x^2} \right|_1 + \lambda_{xy} \left. \frac{\partial^2 \phi}{\partial x \partial y} \right|_1 + \lambda_{yy} \left. \frac{\partial^2 \phi}{\partial y^2} \right|_1 \right) + \\ & h \left(\lambda_{xxx} \left. \frac{\partial^3 \phi}{\partial x^3} \right|_1 + \lambda_{xxy} \left. \frac{\partial^3 \phi}{\partial x^2 \partial y} \right|_1 + \lambda_{xyy} \left. \frac{\partial^3 \phi}{\partial x \partial y^2} \right|_1 + \lambda_{yyy} \left. \frac{\partial^3 \phi}{\partial y^3} \right|_1 \right) \\ & + \mathcal{O}(h^2) \end{aligned} \tag{19}$$

The truncation error of Laplace's equation flux integral using a uniform mesh and the $A00$ discretization scheme is second-order accurate in the sense that the error coefficients in the zero and first order terms are all zero. Moreover, using pure averaging (without adding finite difference correction and/or jump term), the computed Laplacians for the sheared and scaled meshes are first-order accurate, whilst they are zero-order accurate for the stretched, curved and randomly perturbed meshes. These results are consistent with the numerical experiments of Diskin and Thomas[7] and with our own numerical experiments (see Section IV), and does not necessarily imply that the discrete solution error will be less than second order.

Since the number of possible discretization schemes based on combining the choice of averaging, the type of finite difference correction term (if any), and adding or not adding the jump term is too extensive to test comprehensively on general meshes, we wish to eliminate some of the methods that do not perform well even for slightly distorted meshes.

1. Averaging methods

Our numerical tests in Section IV reveal that approximating the face gradient as the average of the gradient of the cells at both sides of it results in a zero-order flux integral for Laplace's equation (Equation 19) for some meshes. We define the truncation error metric of discretization schemes as the L_2 norm of error coefficients in leading order terms of the truncation error. This definition can be written as

$$E_i = \sqrt{\lambda_{xx}^2 + \lambda_{xy}^2 + \lambda_{yy}^2} \tag{20}$$

for a zero-order flux integral. As mentioned earlier, the truncation error of Laplace's equation is zero-order accurate for stretched and curved meshes provided that the face gradient is calculated as the average of two

adjacent cells gradient. Hence, the truncation error metric for each control volume of these two meshes is defined as Equation 20.

To compare the accuracy of averaging methods, a set of analytic tests has been done for the stretched and curved meshes with the aim of omitting the method that does not work well even for these slightly distorted grids. Figure 3a shows E_1(which is the truncation error metric for CV_1) of the stretched mesh computed through various averaging methods for different values of stretching factor. Similarly, Figure 3b shows E_1 for the curved mesh in terms of a for a fixed radius ratio and the aforementioned averaging alternatives. Even though arithmetic averaging and linear interpolation are comparable in terms of truncation error metric values, the truncation error that volume weighted averaging produces is larger for both of contrived meshes. This behavior can be explained by considering the fact that volume-weighted averaging emphasizes the effect of larger control volume although the centroid of the larger triangle is farther than the centroid of the smaller triangle from the face midpoint. This defect has been modified in linear interpolation where the weight of averaging is determined by the distance of the opposite cell centroid to the face midpoint. We conclude that using volume weighted averaging is not a good choice for general unstructured meshes. Based on this conclusion, we eliminate those schemes that use volume weighted averaging for our numerical tests in Section IV.

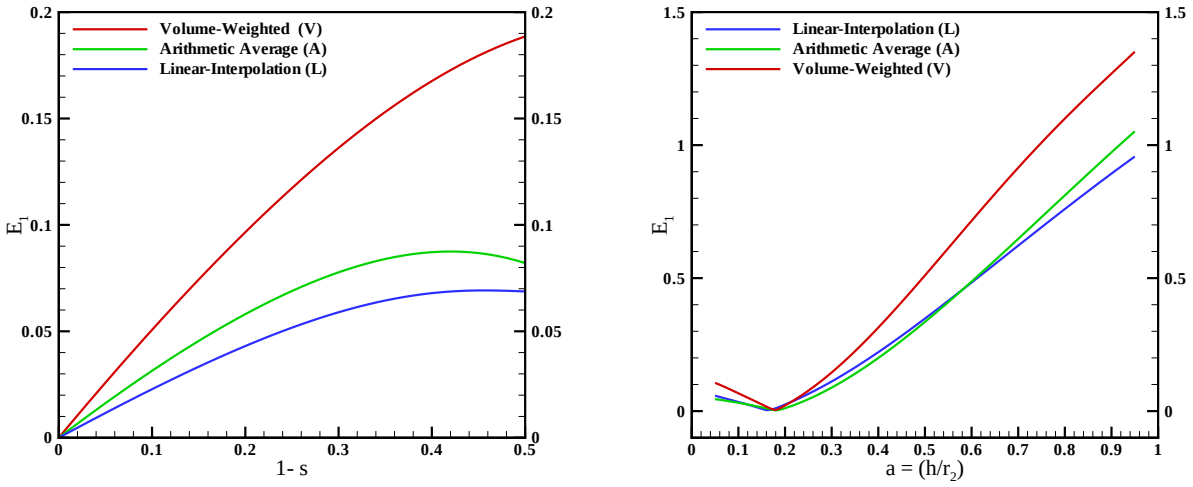

(a) stretched mesh

(b) curved mesh, $R = 1.15$

Figure 3: Averaging methods comparison

2. *Finite difference correction*

In addition to the type of averaging, the choice of finite difference correction term influences the overall accuracy of discretization schemes. Table 1 summarizes different options for setting such a kind of correction term. Some discretization schemes do not use any finite difference term; however, the proposed ways of implementing this term have been widely used by different flow solvers. In this section, an analytic test is conducted to compare the accuracy of proposed finite difference correction terms based on their performance on distorted meshes.

Table 3 shows the order of accuracy of Laplace's equation flux integral for CV_1 of contrived meshes. Four discretization schemes have been utilized that only differ in implementing finite difference correction term. For consistency, linear interpolation is used for the averaging in all schemes. $L00$ does not use any finite difference term while $L0E$, $L0N$ and $L0C$ use such a correction term in edge, face normal and corrected normal directions, respectively. By careful investigation of this table, it is concluded that the face normal direction (corresponding to $L0N$) reduces the order of accuracy of the flux integral in most of the cases. The only exception is the stretched mesh in which all of the correction directions are identical. This result

simply reveals that using finite difference correction term in face normal direction is not an appropriate choice regardless of the magnitude of error coefficients.

	Meshes				
Scheme	Sheared	Scaled	Stretched	Curved	Randomly perturbed
$L00$	$\mathcal{O}(h^1)$	$\mathcal{O}(h^1)$	$\mathcal{O}(h^0)$	$\mathcal{O}(h^0)$	$\mathcal{O}(h^0)$
$L0E$	$\mathcal{O}(h^1)$	$\mathcal{O}(h^1)$	$\mathcal{O}(h^0)$	$\mathcal{O}(h^0)$	$\mathcal{O}(h^0)$
$L0N$	$\mathcal{O}(\frac{1}{h})$	$\mathcal{O}(\frac{1}{h})$	$\mathcal{O}(h^0)$	$\mathcal{O}(\frac{1}{h})$	$\mathcal{O}(\frac{1}{h})$
$L0C$	$\mathcal{O}(h^1)$	$\mathcal{O}(h^1)$	$\mathcal{O}(h^0)$	$\mathcal{O}(h^0)$	$\mathcal{O}(h^0)$

Table 3: Finite difference correction term comparison for distorted meshes

IV. Numerical Tests

The results of the previous section were obtained using a computer algebra system to replace laborious hand calculations. This was possible because the topology of the mesh was regular. For a general unstructured mesh, with its irregular topology, that approach would require separate analysis for each control volume, which is impractical. Therefore, we need to develop a numerical test to assess the performance of discretization schemes in terms of truncation error. In this section, a numerical test methodology is introduced which is employed to compare the truncation error of the Laplacian using various discretization schemes. Those schemes working reasonably well for slightly distorted meshes in Section III are compared for both isotropic mesh and anisotropic mesh test cases.

A. Methodology

To extend our approach to arbitrary unstructured mesh stencils, we write the general discrete form of the flux integral for a linear problem in terms of control volume averages as

$$\widetilde{\nabla^2\phi}_i = \sum_j A_{ij}\overline{\phi}_j \tag{21}$$

where the summation is over control volumes j in the stencil of i. The first key part of our approach is the observation that A_{ij} is one row of the global flux Jacobian. The second key is the ability to calculate that Jacobian explicitly, which our flow solver can do for schemes up to fourth-order accuracy.[8] Now we proceed as we did for the analytic tests, replacing the control volume averages $\overline{\phi}_j$ by expansions involving the solution and its derivatives at the reference point of control volume i, using Equation 6. In computing the sum, we accumulate coefficients of terms in the series expansion of $\widetilde{\nabla^2\phi}_i$. This process is much faster than a single implicit time step for the flow solver, as it requires only a Jacobian calculation and a handful of matrix-vector multiplications. $\overline{\nabla^2\phi}_i$ is found by computing the average of Laplace's equation over control volume i:

$$\begin{aligned}\overline{\nabla^2\phi}_i \;=\; & \left.\frac{\partial^2\phi}{\partial x^2}\right|_i + \left.\frac{\partial^2\phi}{\partial y^2}\right|_i + \left.\frac{\partial^3\phi}{\partial x^3}\right|_i \overline{x}_i + \\ & \left.\frac{\partial^3\phi}{\partial x^2\partial y}\right|_i \overline{y}_i + \left.\frac{\partial^3\phi}{\partial x\partial y^2}\right|_i \overline{x}_i + \left.\frac{\partial^3\phi}{\partial y^3}\right|_i \overline{y}_i + \left.\frac{\partial^4\phi}{\partial x^4}\right|_i \frac{\overline{x_i^2}}{2} \\ & \left.\frac{\partial^4\phi}{\partial x^3\partial y}\right|_i \overline{xy}_i + \left.\frac{\partial^4\phi}{\partial x^2\partial y^2}\right|_i \left(\frac{\overline{x_i^2}}{2} + \frac{\overline{y_i^2}}{2}\right) + \left.\frac{\partial^4\phi}{\partial x\partial y^3}\right|_i \overline{xy}_i + \left.\frac{\partial^4\phi}{\partial y^4}\right|_i \frac{\overline{y_i^2}}{2} + \ldots\end{aligned} \tag{22}$$

So, the difference of $\widetilde{\nabla^2\phi}_i$ and $\overline{\nabla^2\phi}_i$ simply yields the truncation error for each control volume in the same form as Equation 19. Depending on the discretization scheme that is employed for approximating the face gradient, different error coefficients in Equation 19 are obtained. Recalling that discretization schemes that use volume weighted averaging and/or finite difference term in the face normal direction were

omitted based on our analytical tests in Section III, numerical accuracy tests are done for the remaining discretization schemes. These schemes utilize arithmetic averaging or linear interpolation and might have a jump term and/or a finite difference correction term in the edge or corrected normal directions. Note that if the finite difference term is applied in the corrected normal direction, the averaged component (resulting from arithmetic averaging or linear interpolation) will be projected on the tangential direction. Since the flux integral is obtained through Equation 17, the tangential component of the face gradient does not affect the flux integral. Therefore, there will be no significance in choosing the averaging scheme if the corrected normal finite difference term is used.

Based upon the alphanumeric triplet nomenclature defined in Section II, the remaining schemes that are compared for isotropic and anisotropic meshes are $A00$, $L00$, $A0J$, $L0J$, $AE0$, $LE0$, $0C0$ (exactly the same as $AC0$ and $LC0$), AEJ, LEJ and $0CJ$ (ACJ and LCJ).

B. Isotropic grids

As mentioned in Section III, the truncation error of Laplacian for a general unstructured mesh is zero-order accurate. In general, the truncation error for each control volume can be written as

$$TE_i = \left(\lambda_{xx} \left. \frac{\partial^2 \phi}{\partial x^2} \right|_i + \lambda_{xy} \left. \frac{\partial^2 \phi}{\partial x \partial y} \right|_i + \lambda_{yy} \left. \frac{\partial^2 \phi}{\partial y^2} \right|_i \right) + \mathcal{O}(h) \tag{23}$$

in which $\left. \frac{\partial^2 \phi}{\partial x^m \partial y^n} \right|_i$ are second derivatives evaluated at the centroid of control volume i. Considering that an isotropic mesh is used for isotropic solutions, all of the derivatives in Equation 23 have the same order of magnitude, so the truncation error metric is defined as the L_2 norm of zero-order term error coefficients (Equation 20).

To compare the truncation error produced by various discretization schemes, the area weighted average of the error metric is evaluated for interior control volumes. Figure 4 shows two isotropic test cases that are used for comparison. Both of the test cases consist of isotropic triangles with different resolutions in a rectangular geometry.

Using each of the discretization schemes, the truncation error metric distribution can be easily obtained for our test cases. For instance, Figure 5 illustrates the distribution of truncation error metric over interior control volumes of test case 2 using the $A00$ discretization method.

Some of the remaining schemes use a jump term to take into account the solution discontinuity at the face center. A very big challenge in applying the jump term is the choice of the jump term coefficient (α) that influences the flux integral. To address the effect of α on the truncation error, the area-weighted average of error metric resulting from $L0J$ (linear interpolation along with jump term) has been plotted in terms of α for both of the isotropic grid test cases (Figure 6). Even though Nishikawa[6] suggests $\alpha = \frac{4}{3}$ to obtain the most accurate flux integral, our numerical tests reveal that the optimal value for α is $\frac{2}{3}$ in which the average of truncation error metric is minimum. Therefore, we set $\alpha = \frac{2}{3}$ in all of the schemes that utilize the jump term.

Table 4 summarizes the distribution of truncation error metric for the isotropic grid test cases. This table contains minimum, maximum and area-weighted average of error for both of the test cases. Note that minimum and maximum do not necessarily take place at the same control volumes using different discretization schemes. The comparison of area-weighted average error between the $A00$ and $L00$ scheme shows that linear interpolation performs better than arithmetic averaging. Furthermore, adding a jump term along with the optimal coefficient reduces the average of error more than 15 percent. Using a finite difference correction term in the edge direction always reduces the accuracy of the flux integral; however, a finite difference term in the corrected normal direction is comparable with pure averaging. Likewise, adding both the jump term and a finite difference correction term highly increases truncation error coefficients. A concise outcome of comparison between area-weighted average of truncation error metric suggests $L0J$ as the most efficient discretization scheme although it is comparable with $A0J$. Since the implementation of arithmetic averaging is easier than linear interpolation, one might prefer to utilize $A0J$ for diffusive flux approximation of isotropic triangular meshes.

To investigate the magnitude of the difference in the truncation error metric distributions produced by two arbitrary schemes, a statistical analysis has been done to assess the similarity of distributions for each pair of schemes. For this purpose, a chi-square test has been conducted for test case 2. This analysis estimates

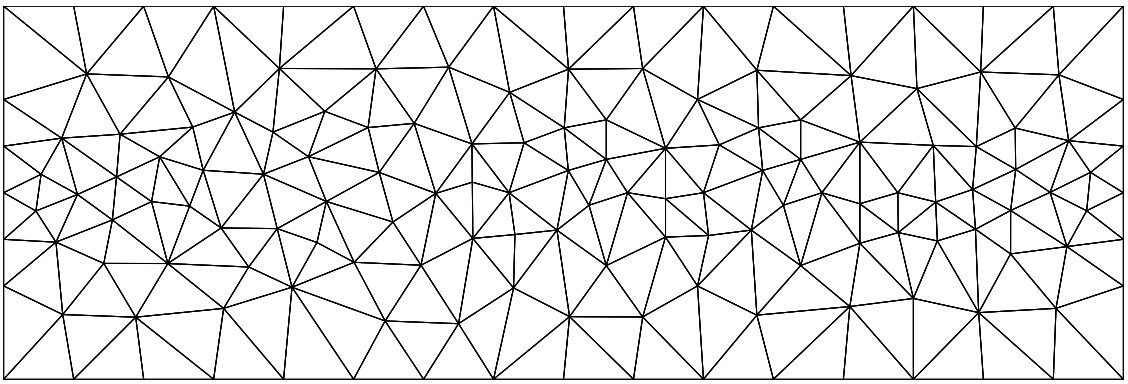

(a) Test case 1 consisting of 153 vertices and 260 triangles

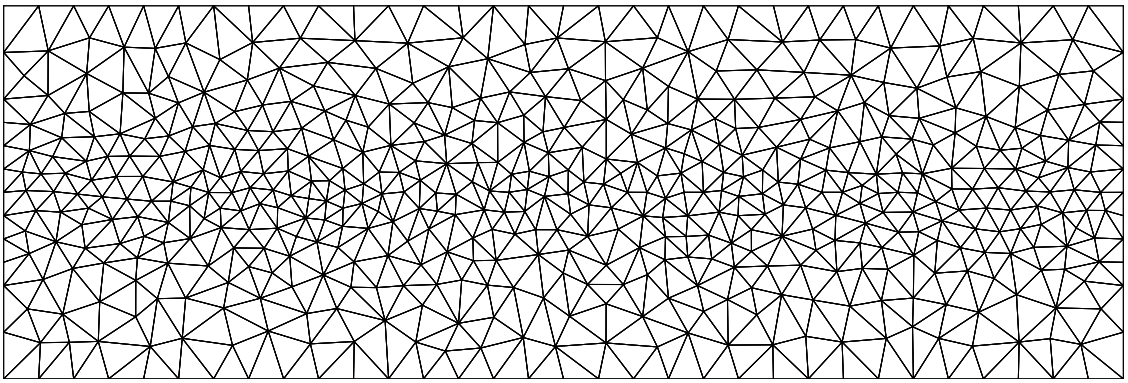

(b) Test case 2 consisting of 559 vertices and 1028 triangles

Figure 4: Isotropic grid test cases

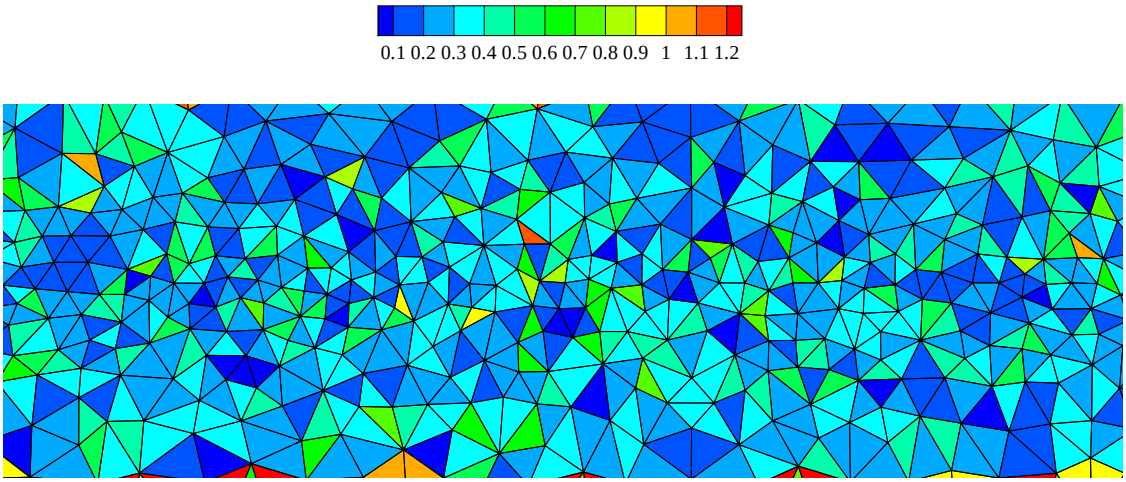

Figure 5: Truncation error metric distribution using $A00$

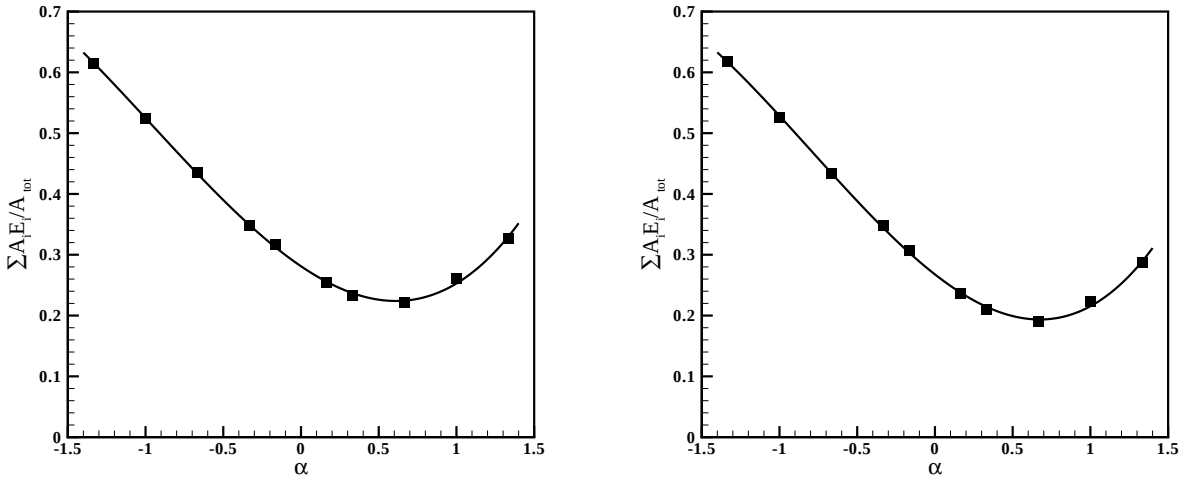

(a) Test case 1

(b) Test case 2

Figure 6: Effect of jump term coefficient on truncation error metric

Scheme	Truncation error metric					
Name	Test Case 1			Test Case 2		
	Min.	Max.	Area-weighted average	Min.	Max.	Area-weighted average
$A00$	0.0588	1.0548	0.3195	0.0310	1.1361	0.2924
$L00$	0.0405	0.8975	0.2826	0.0308	0.9151	0.2697
$A0J$	0.0203	0.9209	0.2403	0.0128	1.0361	0.2017
$L0J$	0.0214	0.8085	0.2222	0.0121	0.8653	0.1899
$AE0$	0.0727	2.2204	0.6060	0.0234	1.8714	0.5024
$LE0$	0.0668	2.2096	0.6131	0.0326	1.906	0.5122
$0C0$	0.0228	1.3208	0.3474	0.0234	1.4917	0.2835
AEJ	0.0489	2.1875	0.5978	0.0142	1.8219	0.4551
LEJ	0.0439	2.1576	0.5999	0.0289	1.8561	0.4603
$0CJ$	0.0441	1.3245	0.4471	0.0449	1.6380	0.3901

Table 4: Truncation error metric distribution summary for isotropic test cases

the probability of the hypothesis that two data sets are drawn from different distributions. Since the chi-square test is applicable only for binned data, we turn our distributions resulting from each discretization scheme into binned samples, by grouping the truncation error metrics into 48 equal ranges. Table 5 gives the probability of difference for each pair of the schemes. According to Table 5, the distributions are nearly identical for those pairs that only differ in type of averaging. This result implies that the type of averaging does not highly affect the overall distribution of truncation error metric for isotropic grids. Also, the $0C0$ scheme is comparable to the uncorrected cell average based schemes $A00$ and $L00$.

Probability of difference									
	$L00$	$A0J$	$L0J$	$AE0$	$LE0$	$0C0$	AEJ	LEJ	$0CJ$
$A00$	0.542	1	1	1	1	0.330	1	1	1
$L00$		1	1	1	1	0.297	1	1	1
$A0J$			0.001	1	1	1	1	1	1
$L0J$				1	1	1	1	1	1
$AE0$					0.012	1	0.827	0.747	1
$LE0$						1	0.982	0.922	1
$0C0$							1	1	1
AEJ								0.010	0.987
LEJ									0.999

Table 5: Probability that error distributions of test case 2 are different

C. Anisotropic grids

To assess the accuracy of different discretization schemes on anisotropic meshes, an irregular anisotropic grid is used as a test case. This kind of mesh is generated on a rectangular domain $(x, y) \in [0, 1] \times [0, 0.1]$ using the procedure that has been described in detail by Diskin *et al.*[3] Figure 7 depicts the anisotropic mesh test case. For generating the test case, the first step is stretching regular rectangular grid with $(N_x+1)\times(N_y+1)$ nodes toward the horizontal line $y = 0.05$. Then, irregularities are introduced by random shifts on interior nodes in vertical and horizontal directions and finally each perturbed quadrilateral is randomly triangulated with one of the two choices for its diagonals.

As for the isotropic case, the truncation error for every control volume of the anisotropic mesh can be written in the form of Equation 23. Recognizing that an anisotropic mesh is used for non-isotropic solution, the values of the second derivatives in Equation 23 do not have the same order of magnitude. Rippa[9] concluded that, for linear interpolation of smooth functions, triangles should be long in the direction where the magnitude of the second directional derivative is small and thin where the magnitude of the second directional derivative is large. Considering the fact that the triangles of our test case in Figure 7 are long in the x-direction and thin in the y-direction, we modify our truncation error metric to take into account the effect of solution anisotropy:

$$E_i = \sqrt{\left(\frac{\lambda_{xx}}{AR_i^2}\right)^2 + \left(\frac{\lambda_{xy}}{AR_i}\right)^2 + \lambda_{yy}^2} \tag{24}$$

As described for the isotropic test cases, the optimal value of jump term coefficient in those schemes that utilize this term should be determined. For that purpose, the area-weighted average of truncation error metric defined in Equation 24 using the $L0J$ method is plotted in terms of α. Figure 8 shows that setting $\alpha = \frac{2}{3}$ gives the minimum value for the average of error. Recalling that this value was the optimal coefficient for the isotropic test cases, we can conclude that jump term coefficient should be set to $\frac{2}{3}$ for all faces regardless of mesh anisotropy.

To investigate the effect of discretization scheme on the truncation error of Laplace's equation using anisotropic meshes, minimum, maximum and area-weighted average of truncation error metrics have been tabulated in Table 6. Comparing the average of error, we see that adding a jump term along with the optimal coefficient improves the accuracy of the flux integral. In fact, this is the best possible choice of discretization

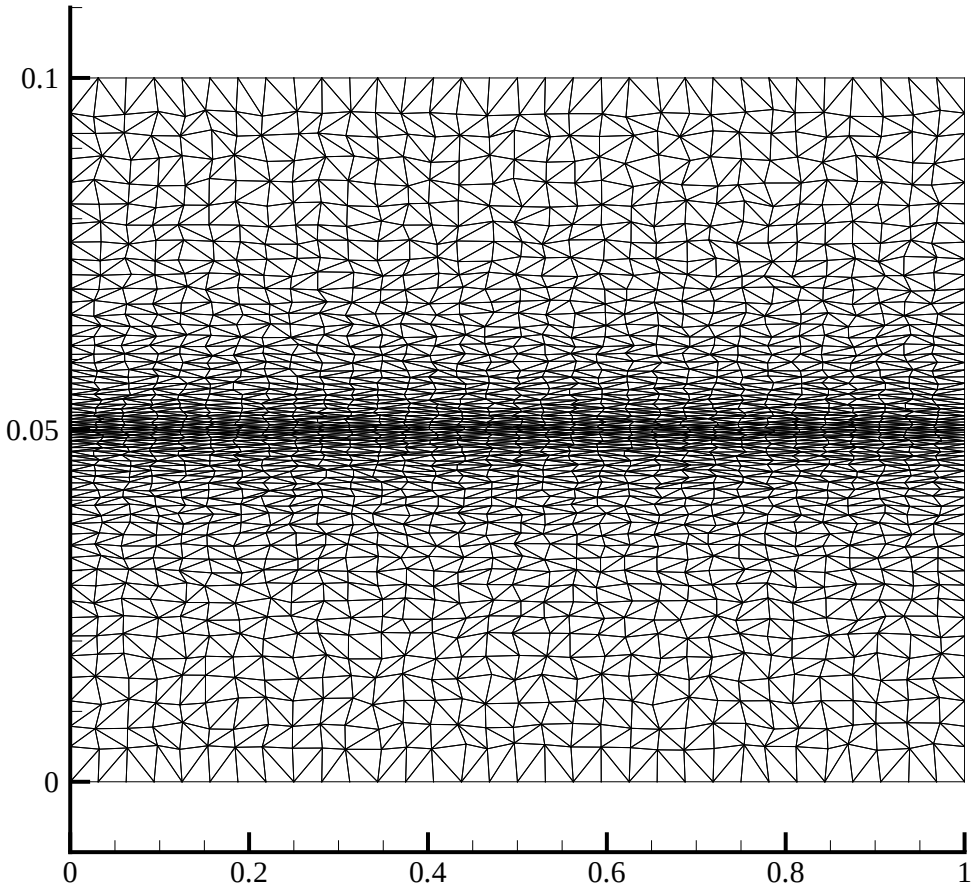

Figure 7: Anisotropic stretched grid with 33×65 nodes

Scheme	Truncation error metric		
	Minimum	Maximum	Area-weighted average
$A00$	0.0136	1.8918	0.3272
$L00$	0.0125	1.1637	0.3576
$A0J$	0.0073	1.4396	0.2521
$L0J$	0.0089	0.8422	0.2639
$AE0$	0.0143	1.8895	0.3275
$LE0$	0.0145	1.1635	0.3578
$0C0$	0.0157	2.2844	0.3399
AEJ	0.0047	1.4392	0.2515
LEJ	0.0101	0.8424	0.2639
$0CJ$	0.0055	2.0013	0.4601

Table 6: Truncation error metric distribution summary for anisotropic test case

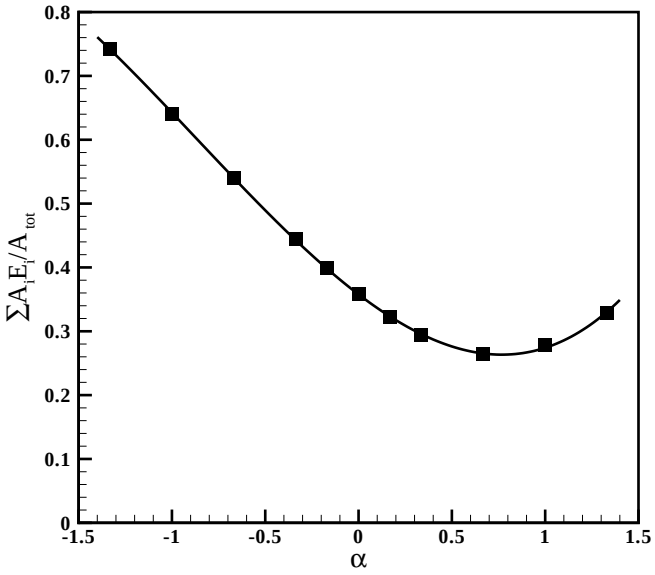

Figure 8: Effect of jump term coefficient on truncation error metric (anisotropic mesh)

scheme for both isotropic and anisotropic meshes. In the meanwhile, using linear interpolation results in a smaller maximum truncation error metric; however, arithmetic averaging produces smaller error average. In contrast to isotropic meshes in which finite difference correction in the edge direction increases the error, this term does not have any significant effect on the truncation error metric for anisotropic meshes. This can be seen by comparing the average of error between $A00$ and $AE0$ or $L00$ and $LE0$.

Probability of difference									
	$L00$	$A0J$	$L0J$	$AE0$	$LE0$	$0C0$	AEJ	LEJ	$0CJ$
$A00$	1	1	1	0.001	1	0.954	1	1	1
$L00$		1	1	1	0.001	1	1	1	1
$A0J$			0.993	1	1	1	0.001	0.996	1
$L0J$				1	1	1	0.989	0.001	1
$AE0$					1	0.967	1	1	1
$LE0$						1	1	1	1
$0C0$							1	1	1
AEJ								0.993	1
LEJ									1

Table 7: Probability that error distributions of anisotropic test case are different

The summary of chi-square test for each pair of discretization schemes tested on anisotropic mesh (Table 7) verifies this conclusion. Similar to the isotropic test case, these results are obtained by turning the truncation error metric distributions into binned data by grouping them into 48 ranges. For example, the probability of difference for distributions of $A00$ and $AE0$ is almost zero. This implies that adding a finite difference correction term in the edge direction does not change the overall distribution of the truncation error metric. This conclusion applies generally to all those pairs that only differ in the presence or absence of the center-to-center edge finite difference correction. To understand why adding a finite difference term in the edge direction does not affect the distribution of truncation error metric, consider the idealized anisotropic triangles depicted in Figure 9. This ideal mesh consists of regular right triangles whose aspect ratios are AR.

Recognizing that the contribution of flux vector determined at edge ab (a very small edge) is negligible in the flux integral at high aspect ratio, two possible geometrical configurations for edges bc and ca have been illustrated in Figures 9a and 9b. In Figure 9a, it is quite straightforward to show that the cosines of θ and γ, the angles between the finite difference correction vectors and corresponding edges, are:

$$cos\,\theta = \frac{AR^2 - 1}{AR^2 + 1} \qquad cos\,\gamma = \frac{AR}{\sqrt{AR^2 + 4}} \tag{25}$$

For large values of AR, these relations can be approximated as

$$cos\,\theta \cong cos\,\gamma \cong 1 - \frac{2}{AR^2} + \mathcal{O}\left(\frac{1}{AR^4}\right) \tag{26}$$

Hence, these two angles are very close to zero for anisotropic mesh with high aspect ratio. This suggests that the finite difference vectors are nearly tangential to edges bc and ca and thus the finite difference correction does not play a significant role in flux integration. Likewise, in Figure 9b, $cos\,\theta$ is evaluated through Equation 25 and the finite difference term has an insignificant effect on the face gradient of edge ca provided that high aspect ratio triangles are used. For this configuration, $\gamma = \frac{\pi}{2}$, so the finite difference term is the only term in the gradient of face bc. Under this condition, the averaged component coming from the least-squares reconstruction is projected on the perpendicular direction to $\vec{r}_{bc}$; this component, which is along edge bc, does not influence the flux integral. Hence, we expect a different flux integral by adding finite difference term in edge direction. Nevertheless, we do not see any remarkable variation in truncation error metric using either $A00$ or $AE0$. The key point is that in computing the cell gradient using the least-squares reconstruction, nearby control volume averages are emphasized by introducing the geometrical weights in Equation 7. For the mesh configuration of Figure 9b, $|\vec{r}_{bc}| \ll |\vec{r}_{ab}|, |\vec{r}_{ca}|$, so the y-component of the computed cell gradient for CV_i is mainly dependent on CV_1 . This suggests that the average of the cell gradients for face bc is approximately equal to finite difference approximation for that face. Therefore, replacing the face normal part of the cell gradient with the finite difference term in the edge direction does not change the truncation error metric distribution for different configurations of anisotropic mesh. Despite the fact that the reasons were described for an idealized mesh, they are easily generalizable to irregular anisotropic grids.

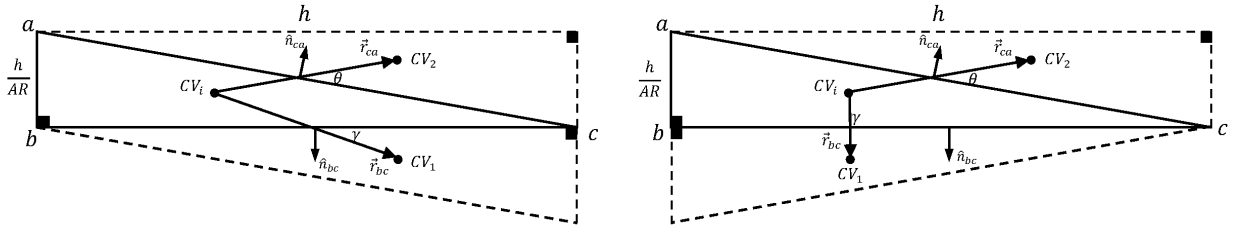

(a) Configuration 1

(b) Configuration 2

Figure 9: Anisotropic mesh configurations

V. Conclusion

The accuracy of different discretization schemes that are widely used for the computation of diffusive fluxes on unstructured meshes have been compared in terms of the produced truncation error. The analysis has been done using a second-order cell-center finite volume approach. The schemes differ in how the cell gradients are computed, the way by which the cell gradients are combined to approximate the face gradient, the presence or absence of a face jump term and the type of finite difference correction term. Analytical and numerical tests have been conducted to assess the accuracy of flux integral for the Laplace's equation as a model of viscous discretization.

The analytical tests have been done using a uniform mesh and distorted meshes coming from perturbation of the uniform mesh. The aim of the analytical tests is to reduce the extensive number of possible discretization schemes for approximating the face gradient. Our analytic tests show that using the least-square method rather than Green-Gauss formulation provided in this paper results in a more accurate cell

gradient. This result was obtained by comparing the truncation error coefficients of the cell gradient for a randomly perturbed mesh. The comparison of the truncation error metric for stretched and curved meshes demonstrates that linear interpolation and arithmetic averaging outperform volume-weighted averaging. In addition, the analytic tests reveal that adding a finite difference correction term in the face normal direction reduces the order of accuracy of the flux integral for most classes of distorted grids. Thus, those discretization schemes that utilize volume-weighted average of the cell gradients and/or finite difference term in the face normal direction can eliminated from consideration for general unstructured meshes.

The numerical tests extend the accuracy experiments to genuinely unstructured meshes. The Jacobian of the flux integral and series expansions of the control volume averages of the solution are used to find the truncation error coefficients. We applied statistical tests to determine whether differences between average values of error are significant. The remaining schemes have been tested for both isotropic and anisotropic grid test cases. Our numerical tests show that linear interpolation performs somewhat better than arithmetic averaging for isotropic grids. Furthermore, adding the jump term along with the optimal jump term coefficient reduces the truncation error considerably. The optimal jump term coefficient is constant regardless of mesh anisotropy. Even though adding finite difference term in center-to-center edge direction does not affect the truncation error for anisotropic meshes, it reduces the accuracy of flux integral for isotropic grids; because this correction, at best, does no harm to accuracy, we recommend that it not be used.

This paper demonstrates that the truncation error analysis is possible for both contrived and general unstructured meshes. The techniques we have developed are applicable in other contexts to analyze error in discretization schemes. In the near term, we will investigate accuracy of schemes for linear (wave equation) and non-linear (Burgers' equation) convective problems. We also intend to study the accuracy of high-order schemes for both convection and diffusion and the effect of various scheme choices for vertex-centered methods.

References

[1]Dimitri J. Mavriplis. Grid resolution study of a Drag Prediction Workshop configuration using the NSU3D unstructured mesh solver. In *Proceedings of the Seventeenth AIAA Computational Fluid Dynamics Conference*, 2005. AIAA Paper 2005-4729.

[2]Andrew W. Cary, Andrew J. Dorgan, and Mori Mani. Towards accurate flow predictions using unstructured meshes. In *Proceedings of the Nineteenth AIAA Computational Fluid Dynamics Conference*, page 17, 2009. AIAA 2009-3650.

[3]B. Diskin, J.L. Thomas, E.J. Nielsen, H. Nishikawa, and J.A. White. Comparison of node-centered and cell-centered unstructured finite-volume discretizations. Part I: Viscous fluxes. In *Proceedings of the Forty-Seventh AIAA Aerospace Sciences Meeting*, 2009.

[4]Carl F. Ollivier-Gooch and Michael Van Altena. A high-order accurate unstructured mesh finite-volume scheme for the advection-diffusion equation. *Journal of Computational Physics*, 181(2):729–752, 2002.

[5]Matthew J. Grismer, William Z. Strang, Robert F. Tomaro, and Frank C. Witzemann. Cobalt: A parallel, implicit, unstructured, Euler/Navier-Stokes solver. *Advances in Engineering Software*, 29:365–373, 1998.

[6]Hiroaki Nishikawa. Beyond interface gradient: A general principle for constructing diffusion schemes. In *Proceedings of the Fourtieth AIAA Fluid Dynamics Conference*, 2010.

[7]B. Diskin and J.L. Thomas. Accuracy analysis for mixed-element finite-volume discretization schemes. Technical Report 2007-08, National Institute of Aerospace, 2007.

[8]Christopher Michalak and Carl Ollivier-Gooch. Globalized matrix-explicit Newton-GMRES for the high-order accurate solution of the Euler equations. *Computers and Fluids*, 39:1156–1167, 2010.

[9]Shmuel Rippa. Long and thin triangles can be good for linear interpolation. *SIAM Journal on Numerical Analysis*, 29(1):257–270, February 1992.